

Development of Cu-E-Glass Fiber Composites by Powder Metallurgy Route

Pallabi Bhuyan*, Harspreet Singh, Lailesh Kumar, Nidhi Sharma, Deepankar Panda, Deepanshu Verma, Syed Nasmul Alam

Department of Metallurgical and Materials Engineering, National Institute of Technology, Rourkela-769008, Orissa, India

*Email: pallabibhuyan92@gmail.com, Phone: +919437678813

Abstract: Cu-E glass fiber composites were developed with different vol. % of E-glass fiber (10, 20, 30 and 40 vol. %) by powder metallurgy route. Both as-received Cu and nanostructured Cu developed by milling as-received Cu powder for 20 h were used to develop various Cu-E-glass fiber composites. The effect of using as-received Cu powder and nanostructured Cu powder on the properties of the various Cu-E-glass fiber composites was analysed. The samples were sintered at 900°C for 1 h in inert atmosphere. The results show good bonding between the matrix and the reinforcement and there is homogeneous distribution of the reinforcement in the matrix. The hardness of the Cu-E-glass fiber composites was found to increase from 0.8 GPa to 2.7 GPa with increase in vol. % of the glass fiber in case of unmilled and from 1.2 GPa to 2.9 GPa for the milled Cu-E-glass fiber composites. The as-milled Cu-E-glass fiber composites shows better densification and sinterability compared to the unmilled Cu-E-glass fiber composites.

Keywords: Wear, Hardness, Density, Reinforcement.

1. Introduction

Metal matrix composites (MMCs) have generated a wide interest in research community because of its high strength, stiffness and fracture toughness. Metal matrix composites are capable of resisting elevated temperature. Most of the metals and alloys could be used as matrices and the reinforcements have to be stable over a range of temperature and should be non-reactive. For high strength applications the matrices require reinforcements having high modulus. The strength to weight ratios of resulting composites can be higher than most of the alloys. Several factors such as melting point, physical and mechanical properties of the composites at various temperatures determine the service temperature of the composites. Composites have been developed with great success by the use of fiber reinforcements in the case of polymer matrix materials. However, due to the limitation of the use of polymer matrices at high temperature there has been an increase in research in the area of metallic matrix composites [1-3].

Over the last several decades, there has been considerable interest in the use of Cu-based metal matrix composites (MMCs). For many applications pure Cu cannot be used because of its low strength. Therefore, improvement in the properties of Cu has become essential for its applications in cutting-edge technological applications. The improvement of mechanical properties of Cu is important for its use in a larger number of fields. Composite materials offer several applications in the field of building aerospace applications, automotive, ship building industry as it has different advantages over other conventional metals. Metal matrix composite (MMCs) is combines both metallic properties such as



toughness & ductility and ceramic properties such as modulus and high strength which possess shear strength provide service at high temperatures. Cu has a density of 8.96 gm/cc. Cu has a melting point of 1085°C and it has a high thermal conductivity ($401 \text{ W.m}^{-1}.\text{K}^{-1}$) and used as a structural material for cooling. It also has high electrical conductivity ($5.96 \times 10^7 \text{ S/m}$). Cu has a Young's modulus of 130 GPa and its tensile strength is 210 MPa. In order to increase its high temperature properties different reinforcements are being used. Glass fibers are among the most versatile industrial materials known today. They are readily produced from raw materials, which are available in virtually unlimited supply. They exhibit useful bulk properties such as hardness, low susceptibility to moisture absorption, resistance to chemical attack, thermal stability and high melting point, as well as desirable fiber properties such as strength, flexibility, and stiffness. Glass fibers are used in the manufacture of structural composites, printed circuit boards and a wide range of special-purpose products. Glass fibers fall into two categories, low-cost general-purpose fibers and premium special-purpose fibers. Over 90% of all glass fibers are general-purpose products. However, several challenges stand in the way of the development of metal matrix composites reinforced with glass fibers such as higher processing temperatures, fiber/matrix bonding, and the ability to produce desired geometries. The final properties of a composite are determined by the fiber content, matrix material, fiber material, fiber orientation, fiber length and by the distribution in the matrix [4-7].

Here Cu-10, 20, 30 and 40 vol. % E-glass fiber composites have been developed by powder metallurgy route using both as received Cu powder and nanostructured Cu powder developed by mechanical milling of the as-received Cu powder in a high-energy ball mill for 20 h. The effect of nanostructured Cu on sinterability and densification of the composites was analysed. The microstructures of the various composites were analysed. The hardness and density of the various composites were determined and the nature of fracture in these composites was analysed.

2. Materials and Methods

Elemental Cu powder having purity > 99 % and average particle size of ~ 400 mesh was procured from LobaChemie. E-glass fibers were procured from Saint Gobain. Green pellets of unmilled Cu and as-milled Cu for 20 h with different volume fractions (10, 20, 30 and 40%) of E-glass fiber were developed by blending the constituents and cold compaction of the samples under a load of 665 MPa in a uniaxial cold compaction machine. Nanostructured Cu powder was developed by milling the Cu powder in a high-energy Fritsch P-5 planetary ball mill. The vials and balls were made of hardened chrome steel. Toluene was used as a process control agent. The ball to powder mass ratio was maintained at 10:1. Samples were collected at an interval of 5 h of milling for analysis of the milled powder. Sintering of the samples was done in tubular furnace at 900°C for 1 h in Ar atmosphere. Hardness of the various composites was determined using a Leco Vickers microhardness tester. Densities of the composites were determined using Archimedes' principle. A JEOL JSM-6480LV scanning electron microscope (SEM) equipped with an INCAPentaFET-x3 X-ray microanalysis system was used. A high resolution transmission electron microscope (HRTEM) JEM – 2100 JEOL with point to point resolution 0.194 nm was used for analysing the milled powder. A Phillips *PANalytical* PW 3040/00 XRD was also used to characterize the milled powder.

3. Result and Discussion

Elemental Cu powder was milled in a high-energy planetary ball mill in order to synthesize nanocrystalline Cu. Mechanical milling is a very effective processing technique for the preparation of nanocrystalline metallic and ceramic powders. It is a solid-state powder processing technique which involves repeated welding, fracturing, and rewelding of powder particles in a high-energy ball mill. Due to the heavy plastic deformation of the particles during milling there was reduction in crystallite size and increase in strain. In a high-energy planetary ball mill, the grinding balls and the powder in the vial are acted upon by centrifugal forces due to the rotation of the vials about its own axis. The supporting disc rotates in the opposite direction. The impact of the balls on the powder leads to the formation of nanostructured powder. The strain in the powder also rises due to milling. The reduction in crystallite size and increase in strain leads to the broadening of the x-ray diffraction peaks as can be seen in Figs.1(a, b).

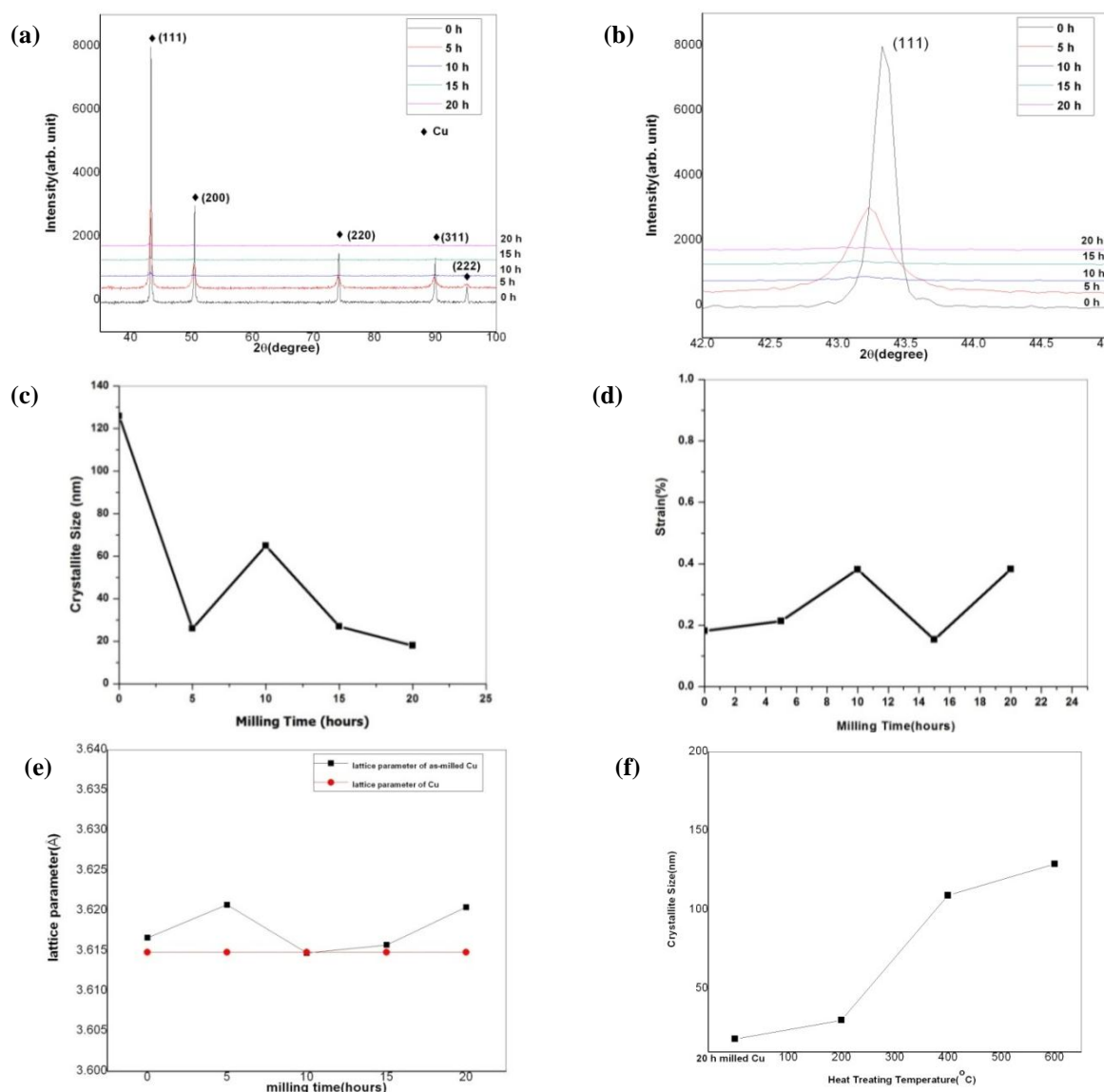


Fig.1 :- (a, b) X -ray diffraction plots of Cu milled for various periods of time and variation of (c) crystallite size (d) r.m.s. strain and (e) lattice parameter of Cu with milling time (f) Variation of crystallite size of the 20 h milled powder with heat treatment temperature.

The x-ray diffraction of Cu powder milled for various durations of time are shown in Fig.1 (a). The various peaks in the x-ray diffraction pattern could be indexed to the different crystallographic planes of Cu. No other peaks could be detected in the x-ray pattern suggesting that there is no contamination from the milling media. Fig.1 (b) presents the (111) peak of unmilled Cu and Cu milled for various periods of time. With increase in milling time broadening of the (111) peak of Cu takes place and its intensity reduces. The (111) peak of Cu at 43.3° after 5 h of milling shows shift towards the lower 2θ angle. The shift of the peak towards the lower 2θ angle is possibly due to the increase in lattice parameter of Cu after 5 h of milling. The lattice parameter variation of Cu with milling time in Fig.1 (e) also presents slight increase with milling time. Beyond 5 h of milling the (111) peak of Cu shows significant broadening as can be seen in Fig. 1(b). Voigt's method was used for calculating the crystallite size of the milled Cu powder from the x-ray diffraction plot using the most intense (111) peak. After 20 h of milling the crystallite size of Cu was found to be 18 nm (Fig.1(c)). There is a gradual drop in the crystallite size with milling time. From Fig. 1(c) it is evident that Cu could be reduced to nanometric dimension within 5 h of milling. Cold welding was also evident between 5 to 10 h of milling which led to the increase in crystallite size. There is a gradual increase in the lattice strain due to severe deformation of the milled powder and strain reaches a maximum value after 20 h of

milling when the crystallite size is smallest (Fig.1 (d)). Fig. 1(f) presents the growth in crystallite size of Cu when the 20 h milled Cu powder is heat treated at various temperatures for 1 h. It shows that the crystallite size of Cu grows to beyond 100 nm after heat treatment at 400°C for 1 h. Therefore at the sintering temperature of 900°C chosen for the deployment of the composites here the crystallite size of Cu is above 100 nm. However the fine size of the milled Cu powder could lead to better sinterability and densification of the composites. This is why the 20 h as-milled Cu powder has been also used for the development of the composites to see the effect of fine sized Cu powder on the properties of the composites [8-11].

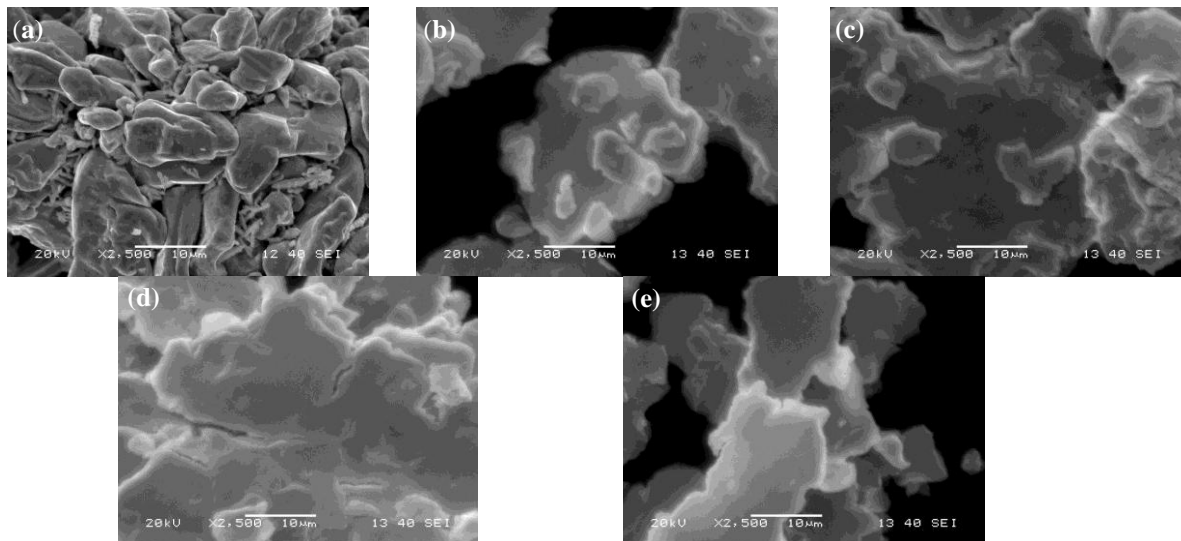


Fig.2:- SEM images of (a) unmilled Cu, Cu milled for (b) 5 h (c) 10 h (d) 15 h (e) 20 h

Figs.2 (a-e) presents the SEM images of Cu powder milled for various periods of time. Due to the ductile nature of Cu it was possible to flatten the Cu particles. The Cu particles which were initially spherical in shape had a flake like shape after 5 h of milling. After 15 h of milling they had a characteristic layered microstructure with very fine lamellar spacing (Fig. 2(d)). Thickening of the plates due to coldwelding between the plates leads to increase in the average particle size of the powder which was seen after 10 h of milling (refer Fig. 1(c)).

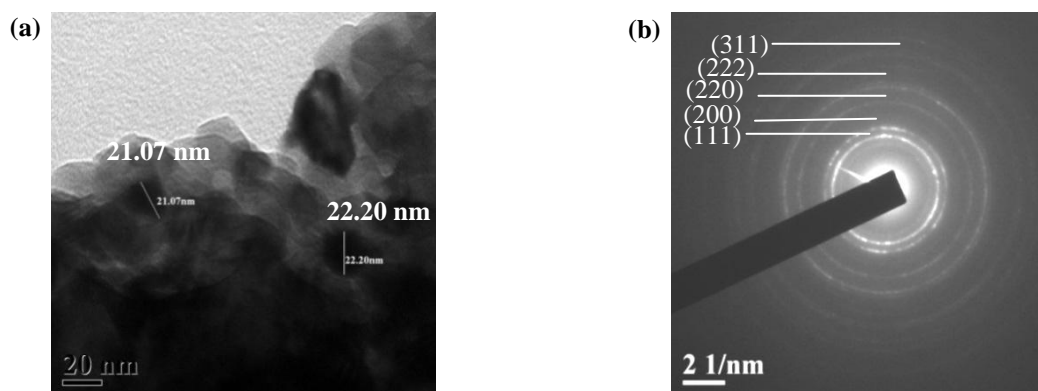


Fig.3 :- (a) HRTEM images and (b) SAD pattern of 20 h milled Cu

The HRTEM image of the 20 h milled Cu powder in Fig.3 (a) indicates that powder has been reduced to nanometric dimension after high-energy milling for 20 h. The SAD pattern in Fig.3 (b) shows complete ring pattern which suggests that the 20 h milled Cu powder has nanometric dimension. The ring patterns could be indexed to the various crystallographic planes of Cu. The particle size analysis of the Cu powder milled for various periods of time was done by particle size analyser. Figs.4 (a, b) shows the particle size analysis for unmilled Cu and 20 h milled Cu powder. It should be noted that size distribution of both the unmilled Cu and the 20 h milled Cu is bimodal in nature showing peaks at

less than 1 μm and higher than 10 μm . There is presence of very fine Cu powder particles having size less than 1 μm in both the unmilled Cu powder as well as the 20 h milled Cu powder although the volume fraction of this fine sized powder is very low in both the unmilled and the 20 h milled Cu powder.

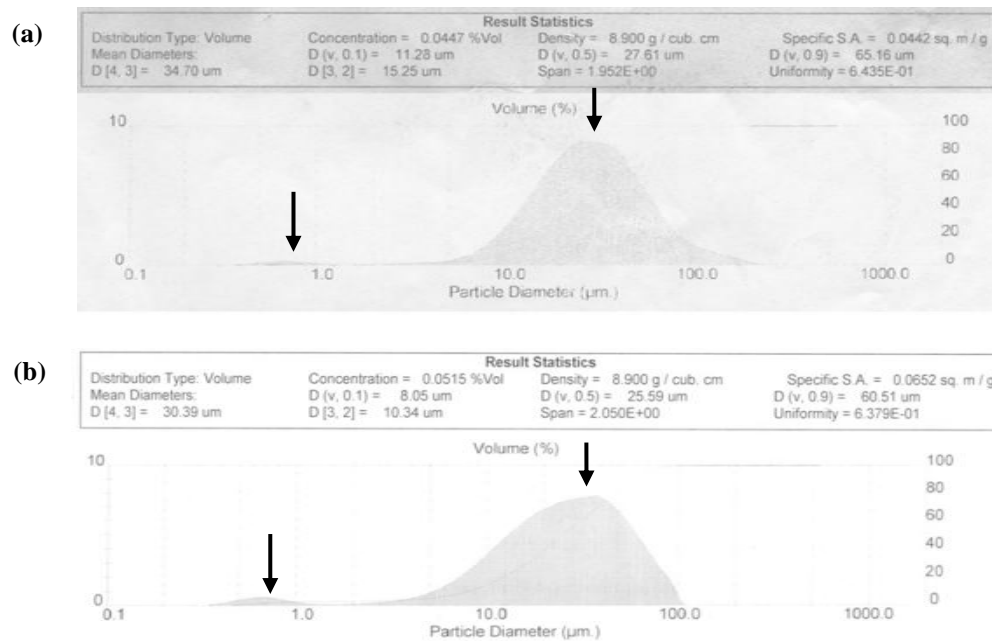


Fig.4:- Particle size analysis for (a) unmilled Cu and (b) 20h milled Cu powder

The average size of the particles was found to be 25.59 μm after 20 h of milling. Table 1 shows the particle size analysis of pure elemental Cu after various periods of milling time. The results show that there is a sudden increase in particle size after 5 h of milling. This is possibly due to the cold welding effect as Cu is soft and ductile material. Beyond 5 h of milling the size of the particles gets reduced due to fracture of the particles which leads to size reduction. The lowest particle size of 25.59 μm is attained after 20 h of milling [12-14].

Table 1:- Particle size analysis of pure Cu at different milling time

Milling Time (hours)	Average Particle Size, D(v,0.5) (μm)
0	27.61
5	57.36
10	35.72
15	25.91
20	25.59

E-Glass fibers are the most widely used glass fibers as reinforcement in the composites. E-glass fibers are alumina-borosilicate glass with less than 1 wt. % alkali oxides and are mainly used for glass-reinforced plastics. E-glass or electrical grade glass was originally developed for use as insulators for electrical wiring which was later found to have excellent fiber forming capabilities and is now used widely as the reinforcing phase in composites and is commonly known as fiber glass. E-glass fibers exhibit useful bulk properties such as hardness (6000 MPa), dimensional stability, resistance to chemical attack and strength. Its density is 2.58 gm/cc. Its tensile strength is 3500 MPa and its Young's modulus is 85 GPa. It has a compressive strength of 5000 MPa [15].

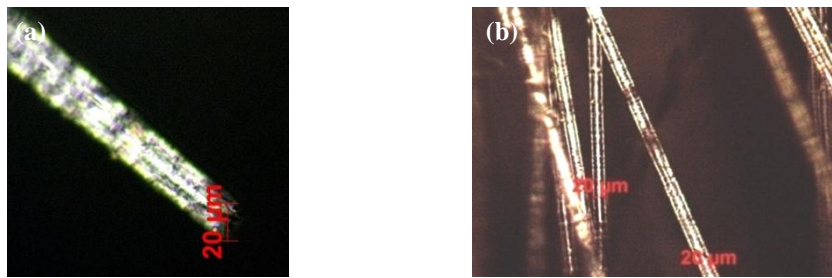


Fig.5 (a, b):- Optical images of E-glass fiber used in the composites

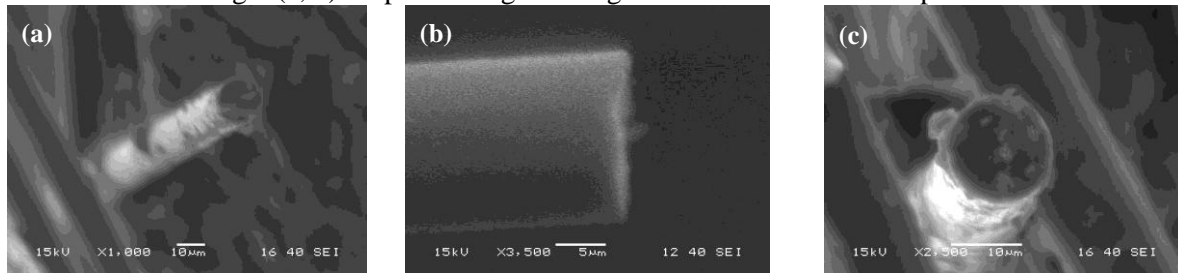
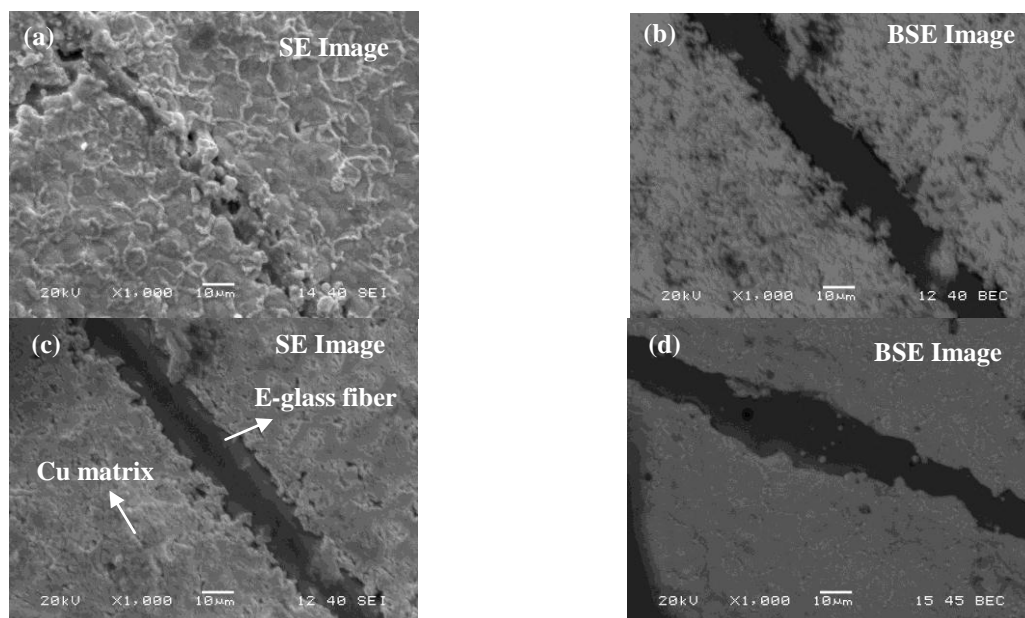


Fig.6 (a-c):- SEM image of E-glass fiber used in the composites

Fig.5 and Fig.6 shows the optical and SEM images respectively of the E-glass fiber used as reinforcement in the Cu-E-glass fiber composites. The diameter of the fibers are $\sim 20\ \mu\text{m}$. Tensile test of the fiber was carried out in order to find out the mechanical properties of the fibers. The fiber shows brittle fracture with elongation to failure of 4.134 %. The elongation to failure for the E-glass fiber is very low as compared to that of ductile metals. E-glass fiber is highly brittle and shows almost flat fracture surface as can be seen from the SEM images in Fig 6. The E-glass fiber shows 100% recovery when stressed below the point of rupture. The tensile strength of a single E-glass fiber was found to be $\sim 2224\ \text{MPa}$.



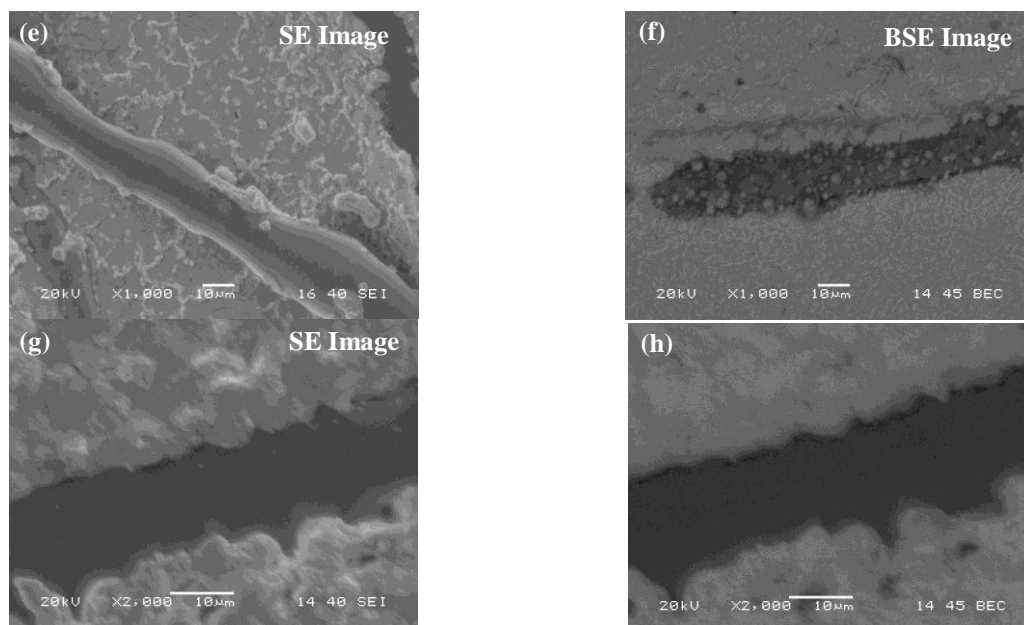


Fig. 8:- SEM image of (a, b) unmilled Cu-10 vol. % E-glass fiber (c, d) unmilled Cu-20 vol. % E-glass fiber (e, f) unmilled Cu-30 vol. % E-glass fiber (g, h) unmilled Cu-40 vol. % E-glass fiber composites sintered at 900°C for 1h

Fig.8 presents the microstructure of various sintered unmilled Cu-E-glass fiber composites developed containing different vol. % of E-glass fiber sintered at 900°C for 1 h in Ar atmosphere. From the microstructural analysis it is evident that the glass fibers are randomly oriented in the Cu matrix and the glass fibers shows very good bonding with the Cu matrix. Back scattered SEM images also show very good wettability of Cu with E-glass fiber. A homogeneous distribution of the reinforcement in the Cu matrix could also be seen. Very few pores could be seen in the Cu matrix as well as the interface of the glass fiber and the Cu matrix [16-18].

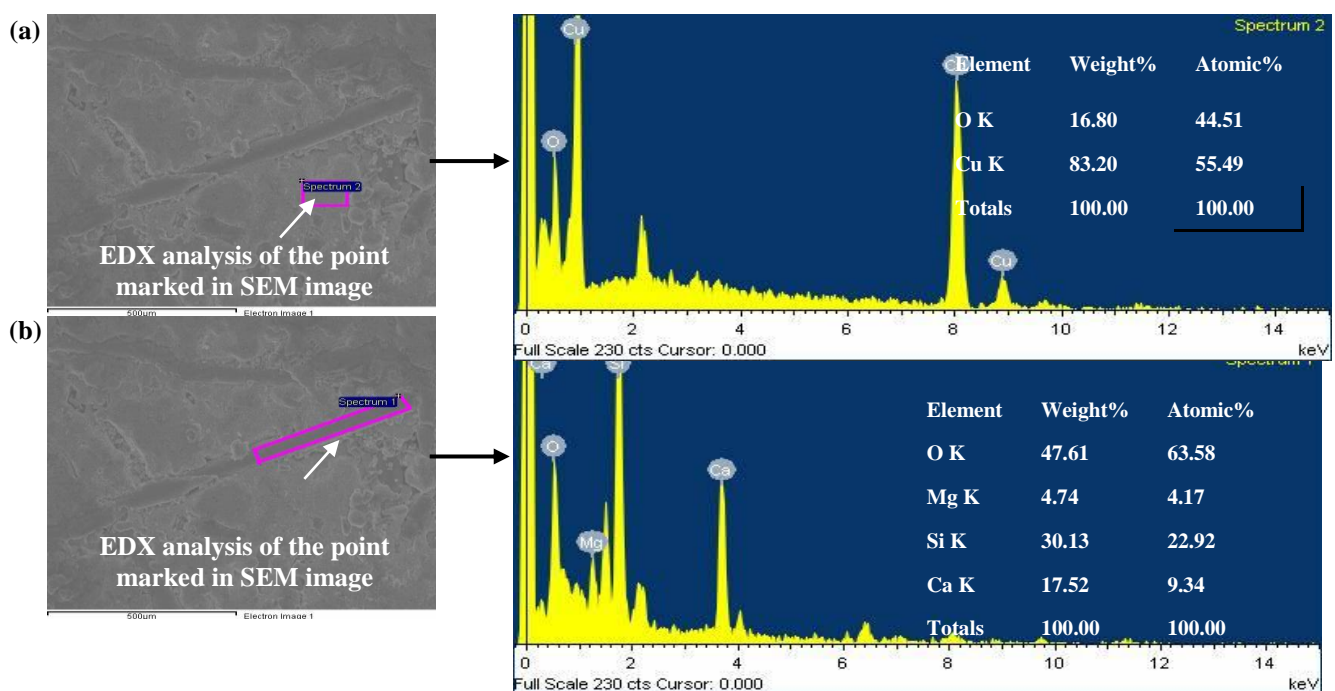


Fig.9 (a, b):- EDX analyses of sintered unmilled Cu-40vol. % composite

Fig.9 presents the EDX of both the reinforcement and the matrix phase in unmilled Cu-40 vol. % composite. The EDX analysis of the Cu matrix in Fig. 9(a) presents the presence of oxygen in the matrix. This is possibly due to the unavoidable oxygen present in the furnace during sintering. The EDX analysis of the E-glass fiber in Fig.9 (b) indicates presence of element like Mg (4.17 at. %), Ca (9.34 at. %), Si (22.92 at. %) and O (63.58 at. %).

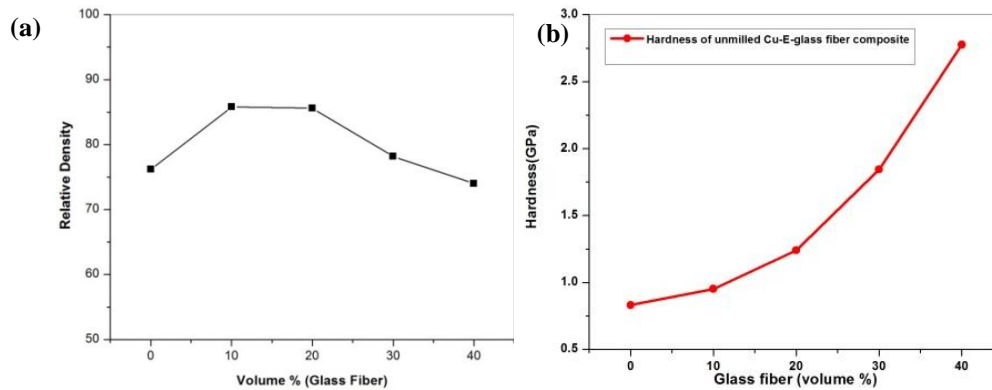
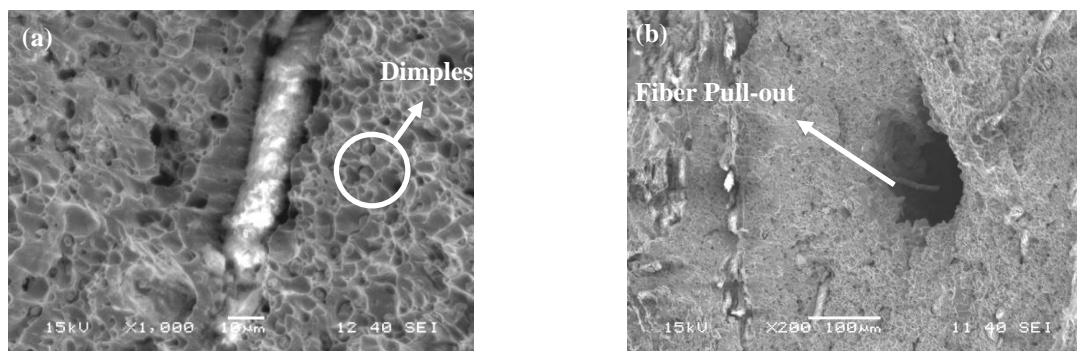


Fig.10:- (a) Variation of (a) relative density (b) hardness of various sintered unmilled Cu-E-glass fiber composites

Fig.10 (a) presents the variation of relative density of unmilled Cu-E-glass fiber composite containing different vol. % reinforcement. The relative density increases initially with increase in the content of E-glass fiber in the composite but it showed slight decreases when higher vol. % of glass fiber was added. It should be noted that a high vol. % of glass fiber could lead to lower theoretical density of the Cu-E-glass fiber composite as compared to that of pure Cu as the density of the E-glass fiber is 2.58 gm/cc and that of Cu is 8.96 gm/cc. Highest relative density of 85.8 % could be achieved in the case Cu-10 vol. % E-glass fiber composite. Fig.10 (b) shows the variation of hardness with the addition of E-glass fiber in the unmilled Cu-E-glass fiber composites. The hardness of the Cu-E-glass fiber composites increases with the increase in vol. % of glass fiber in the composite. This is due to the strengthening of the Cu matrix by the glass fiber. The fracture surfaces of the various composites fractured by impact were also analysed under SEM. The fracture surface of unmilled Cu-10 vol. % E-glass fiber composite in Fig.11 (a) presents the presence of dimples in the Cu matrix suggesting ductile fracture of the Cu matrix. E-glass fibers could be seen embedded in the Cu matrix.



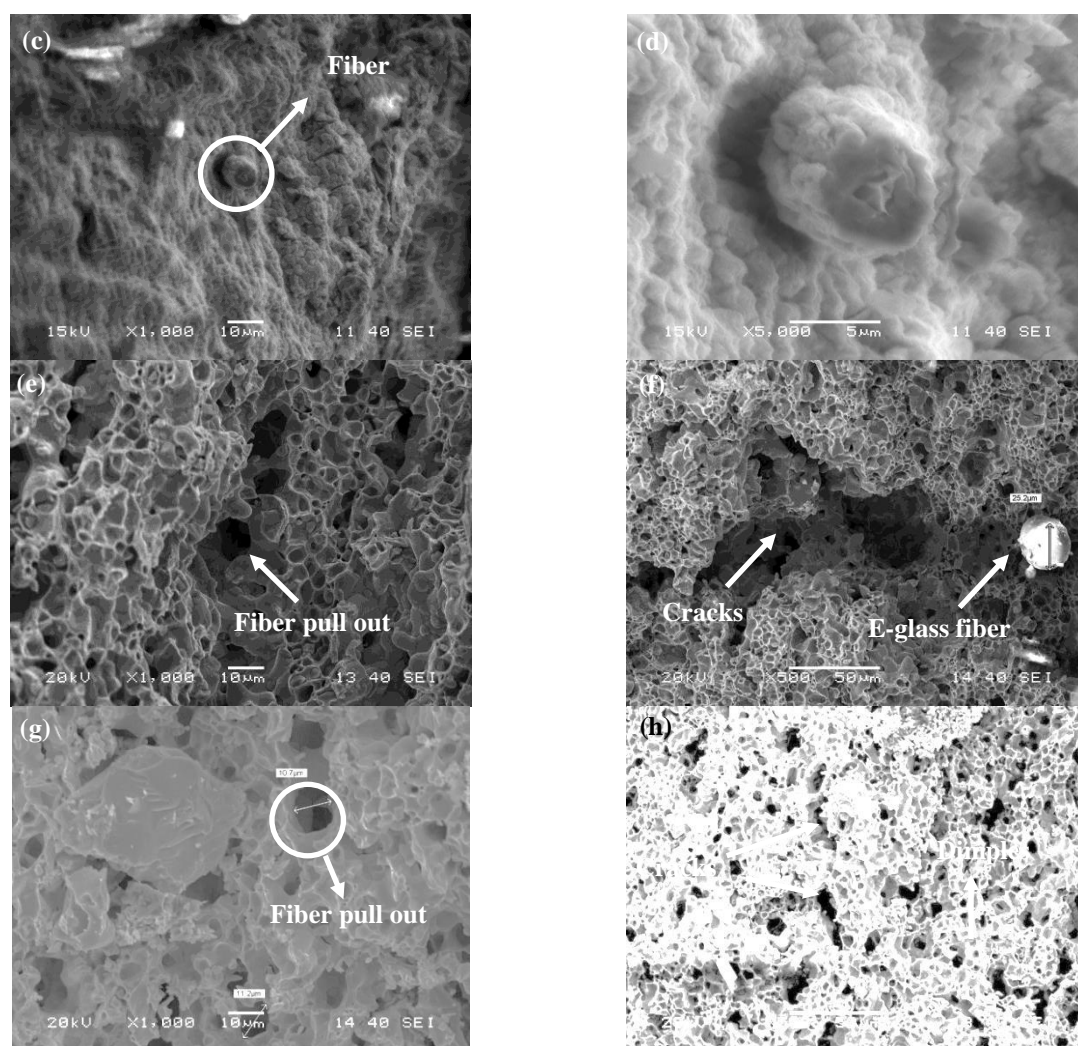


Fig.11:- SEM image of the fracture surface of (a, b) unimilled Cu- 10 vol. % E-glass fiber (c, d) unimilled Cu- 20 vol. % E-glass fiber (e, f) unimilled Cu- 30 vol. % E-glass fiber (g, h) unimilled Cu- 40 vol. % E-glass fiber composite

The SEM image in Fig.11 (b) presents fiber pull out in the fractured surface of the unimilled Cu-10 vol. % E-glass fiber composite. This is possibly due to the lower load bearing capacity as the vol. % of the glass fiber in the composite is very low. Higher stress on each fiber leads to pull-out of the fiber. The stress on the fiber also leads to plastic deformation of the Cu matrix around the fiber. The fiber embedded in the Cu matrix tries to restrict the plastic deformation as is visible from the SEM image. Figs.11(c, d) are the SEM images of the fracture surfaces of unimilled Cu-20 vol. % E-glass fiber composite. From the SEM images it is clear that the nature of fracture in the Cu matrix is ductile whereas the E-glass fiber undergoes brittle fracture. The fractured E-glass fibers have Cu adhered to its surface indicating good wettability and bonding between the Cu matrix and the glass fiber. Figs.11 (e, f) are the SEM images of the fracture surfaces of unimilled Cu-30 vol.% of E-glass fiber composite. The SEM images show ductile nature of fracture in the Cu matrix and brittle fracture of the glass fibers. The SEM images show pull-out of the glass fiber. The SEM images also show the presence of higher amount of pores in the sample. It can be seen from the variation of relative density of various sintered unimilled Cu-E-glass fiber composites in Fig. 4.10(a) that the relative density of the unimilled Cu- 30 vol. % E-glass fiber composite (78.2 %) and Cu- 40 vol. % E-glass fiber composite (74 %) are less than the relative density of unimilled Cu- 20 vol. % E-glass fiber composite (85.8%). Addition of E-glass fiber beyond 20 vol. % has led to a large decrease in the relative density of the composite suggesting the presence of larger volume fraction of pores in the composites containing higher vol. % of E-glass fibers. Addition of glass fiber beyond 20 vol. % leads to poor sinterability and densification of the composites. The large volume of pores has led to the crack in these composites during the tensile

test. The SEM images of Cu 30, 40 vol. % E-glass fiber composites in Figs. 11(e, f) and Figs. 11(g, h) show a large number of crack. Figs.11 (g, h) show the fracture surface of unmilled Cu-40 vol.% of E-glass fiber composite. The Cu matrix shows dimples on its fracture surface which suggests the ductile fracture. Several cracks can be seen clearly in the Cu matrix [19-21].

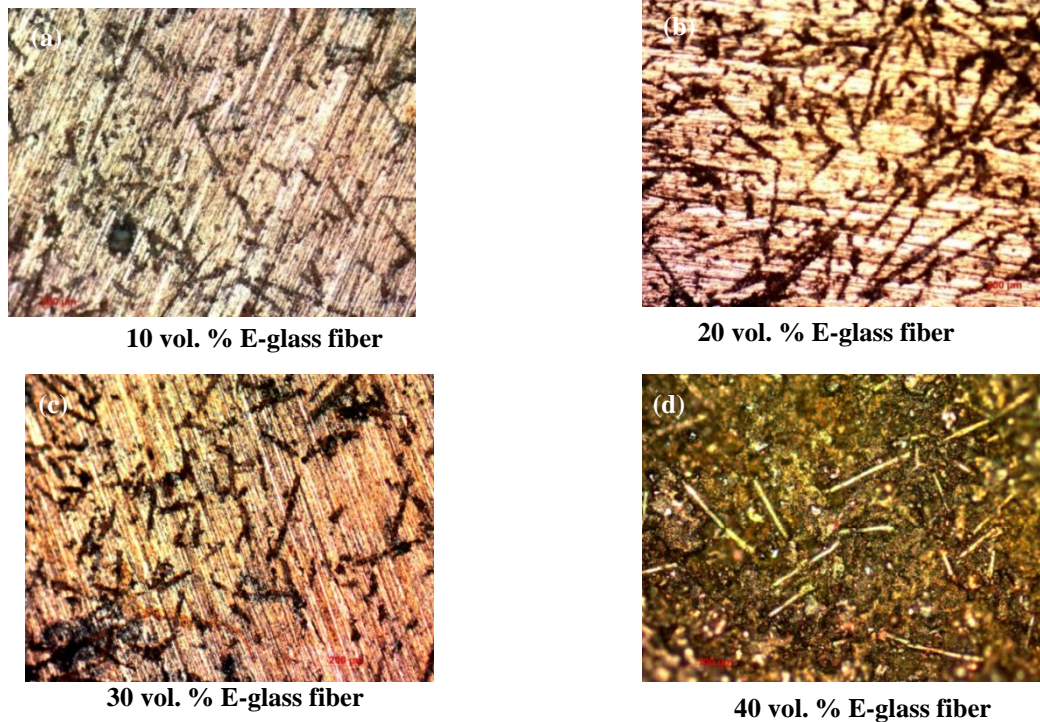


Fig.12 (a-d):- Optical micrographs of as-milled Cu-E-glass fiber composites containing different vol. % of E-glass fiber as reinforcement (10, 20, 30 and 40 vol. %).

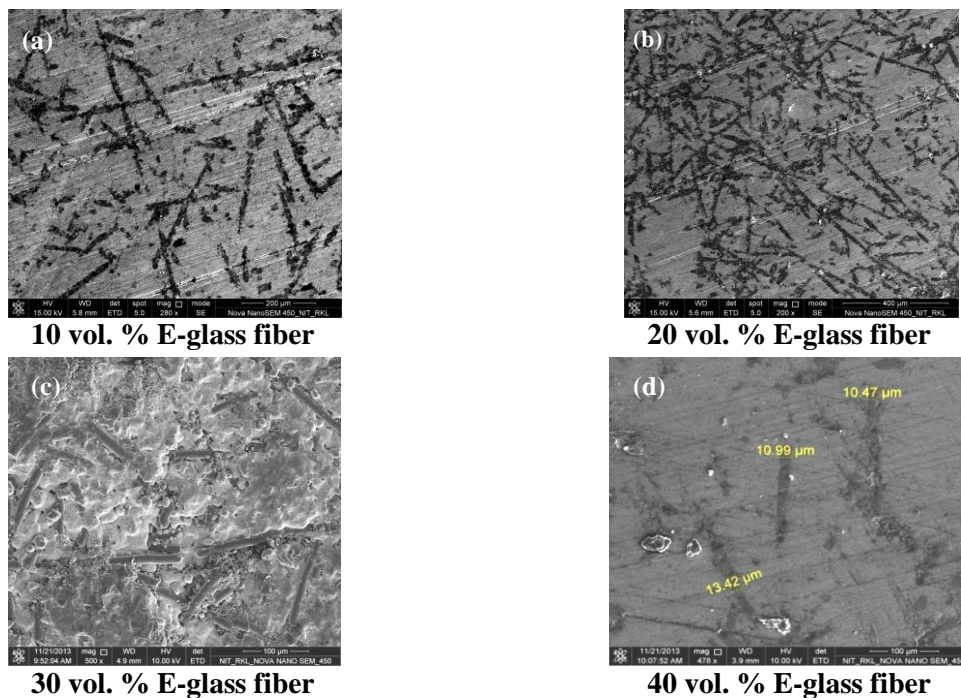


Fig.13:- (a-d) SEM images of as- milled Cu-E-glass fiber composites containing different vol. % of E-glass fiber as reinforcement (10, 20, 30 and 40 vol. %).

From Figs.12 (a-d) it is evident that there is a homogenous dispersion of glass fibers throughout the Cu matrix. It is clearly seen that fibers are embedded in the Cu matrix. SEM images for as-milled Cu-E-glass fiber composites in Figs.13 (a-d) also show the random distribution of reinforcements in the Cu matrix. The SEM images show good wettability of Cu and the E-glass fiber. There is strong adhesion between the Cu matrix and the glass fibers. Comparing the SEM images in Fig.8 of unmilled Cu-E-glass fiber composites and the SEM images in Fig.13 of as-milled Cu-E-glass fiber composites the glass fibers seem more embedded in the Cu matrix and there seems to be a better sinterability in the case of milled Cu-E glass fiber composites. This is also evident from the comparison of the relative densities of the unmilled Cu-E-glass fiber composites and the as-milled Cu-E-glass fiber composites shown in Fig. 10(a) and Fig. 14(a) respectively. The as-milled Cu-E-glass fiber composites show higher relative densities as compared to the unmilled Cu-E-glass fiber composites.

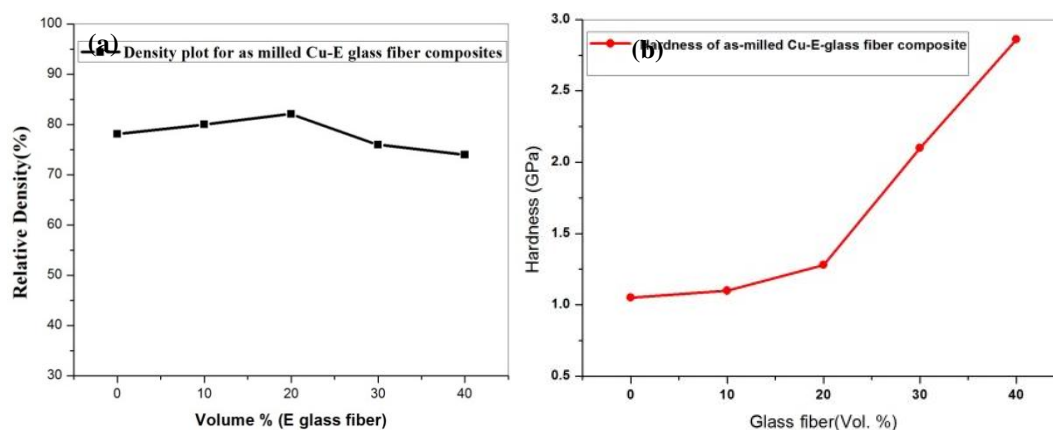


Fig 14:- Variation of (a) relative density (b) hardness of various sintered as-milled Cu-E-glass fiber composites

In as-milled Cu-E-glass fiber composites 20 h milled Cu powder has been used for the development of the composites. The 20 h milled Cu powder is nanocrystalline in nature and as a result has led to better sinterability and densification as shown in Fig.14 (a). Cu has a melting temperature of 1083°C. Nanocrystalline Cu has higher surface area per unit volume and this could reduce the melting point of nanocrystalline Cu. This is why as-milled Cu possibly softens at the sintering temperature of 900°C and results in better sinterability and densification compared to unmilled Cu-E-glass fiber composites. Fig.14 (b) presents variation of microhardness of the various composites with the addition of glass fibers in the as-milled Cu-E-glass fiber composites. The hardness of the composites shows a gradual increase with increase in the content of E-glass fiber in the composites. Comparing the hardness of the unmilled Cu-E-glass fiber composites and as-milled Cu-E-glass fiber composites in Fig.10 (b) and 14(b) respectively it can be seen that the as-milled Cu-E-glass fiber composites possess better hardness. This is due to the better densification of the as-milled Cu-E-glass fiber composites during sintering at 900°C for 1 h.

The SEM images of the fracture surface of as-milled Cu-E-glass fiber composites fractured by impact are shown in Fig.15. The fracture surface in Figs.15 (a, b) shows dimples in the Cu matrix which suggests the ductile nature of fracture of the Cu matrix. It can also be seen that fibers are embedded inside the Cu matrix and has good binding with the matrix. The SEM image shown in Fig.15 (b) clearly shows the brittle fracture of E-glass fiber. The fracture surface of the glass fibers are flat and suggest the brittle nature of their fracture. The glass fibers are well embedded in the Cu matrix and there is good wettability and adhesion between the Cu matrix and the glass fibers.

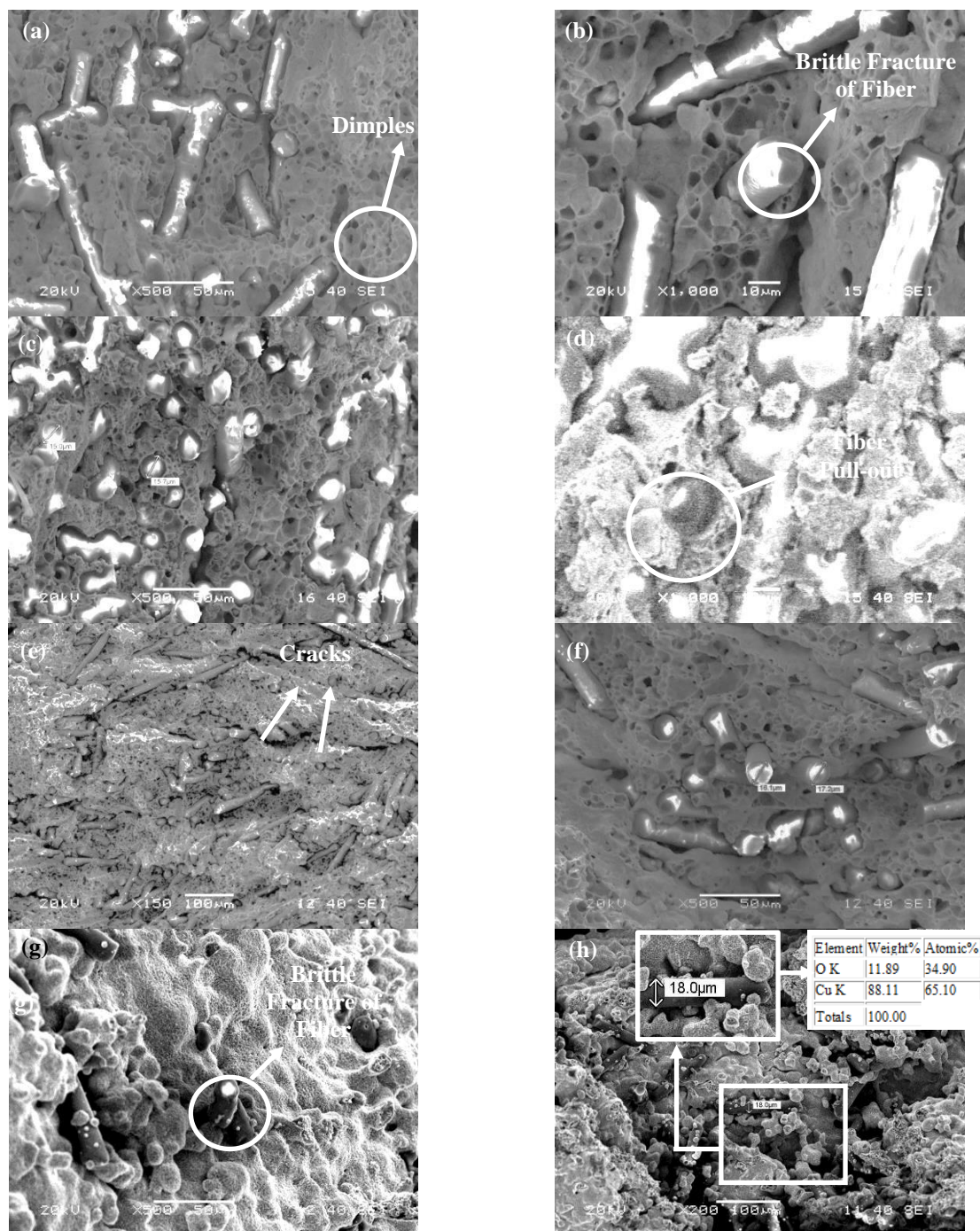


Fig.15:- SEM image of the fracture surface of (a, b) as-milled Cu- 10 vol. % E-glass fiber (c, d) as-milled Cu- 20 vol. % E glass fiber (e, f) as-milled Cu- 30 vol. % E- glass fiber (g, h) as-milled Cu- 40 vol. % E- glass fiber composites. Inset images in Fig. (h) show the magnified image of a section of the SEM image and the EDX of agglomerated Cu particle

Figs. 15 (c, d) presents SEM image of as-milled Cu-20 vol.% E-glass fiber composites. The fibers and the Cu matrix show good bonding between them and the fibers are firmly held in the Cu matrix. There is a random distribution of fibers inside the Cu matrix. Fiber pull-out can be seen in Fig.15 (d). Figs.15 (e, f) presents the SEM images of the fracture surface of as-milled Cu-30 vol.% E-glass fiber composite. The fibers show good interfacial integrity with the Cu matrix. Cracks could be seen in the Cu matrix. Comparison of the SEM images in Fig.11 and Fig.15 shows that in the case of as-milled Cu-E-glass fiber composite there are fewer numbers of pores and cracks in the Cu matrix as compared to the unmilled Cu-E-glass fiber composite. This is possibly due to better sinterability and densification in the case of as-milled Cu composite as compared to the unmilled Cu composite. The

fracture surfaces of the unmilled Cu-E-glass fiber composites show a large number of pores. Plastic deformation in the Cu matrix due to the stress on the fiber during could be seen in the unmilled Cu-E-glass fiber composite (refer Fig. 11(a)). However, such plastic deformations could not be seen in the as-milled Cu-E-glass fiber composites. This suggests stronger bonding between the glass fibers and the Cu matrix in the case of as-milled Cu-E-glass fiber composites. This is due to the better sinterability and densification of the as-milled Cu-E-glass fiber composites. Comparison of the relative densities of unmilled Cu-E-glass fiber composites and as-milled Cu-E-glass fiber composites in Fig. 10 (a) and Fig. 14(a) clearly shows higher relative densities in the case of as-milled Cu-E-glass fiber composites. Figs.15(g, h) presents the SEM image of the fracture surface of as-milled Cu-40 vol.% E-glass fiber composite. The SEM images clearly show Cu adhered to the E-glass fiber surface. The brittle fracture of the glass fiber could be clearly seen in Fig.15 (g). In the case of as-milled Cu- 40 vol. % E- glass fiber composite a large number of Cu rich spherical particles could be seen (refer Fig. 15(h)). This is possibly due to the agglomeration of finer Cu particles which tend to come together to form larger particles and thereby reducing the surface area per unit volume. This was not seen in the case of unmilled Cu composites (Fig.11). This is possibly due to the Gibbs-Thomson effect which predicts that nanoparticles of radius r dissolve at lower electrochemical potentials than bulk materials and thereby decreasing the surface area per unit volume ($1/r$). The Gibbs-Thomson effect is seen due to the reduction of local chemical potential caused by nanoscale curvature [22-24].

4. Conclusion

1. Milling of elemental Cu powder for 20 h led to the formation of nanostructured Cu. The crystallite size of Cu after 20 h of milling was found to be around 18 nm. There is a gradual increase in the lattice strain with milling time due to severe deformation of the milled powder and the strain reaches a maximum after 20 h of milling when the crystallite size is smallest.
2. The hardness values of Cu-E-glass fibre composites increase with increase in vol. % of E-glass fiber in the composite both in the case of milled and unmilled Cu-E-glass fiber composites. The maximum hardness of 2.86 GPa was found in the case of as-milled Cu-40 vol. % E-glass fiber composite.
3. As-milled Cu-E-glass fiber composites shows better densification and sinterability compared to the unmilled Cu-E-glass fiber composites due to the finer size of Cu particles in the milled Cu powder. Better densification and sinterability has also led to higher hardness in the case of milled Cu-E-glass fiber composites.

Acknowledgement

We would like to thank the staff in the SEM and XRD laboratories at the National Institute of Technology-Rourkela, India. The authors would also like to thank the Central Research Facility, Indian Institute of Technology Kharagpur, for allowing them to analyze the samples in the HRTEM laboratory.

References

- [1] B. Harris, Engineering Composite Materials, London, IOM (1999).
- [2] D. Hull and T. W. Clyne, An Introduction to Composite Materials, New York, Cambridge University Press (1996).
- [3] F. L. Matthews and R. D. Rawlings, Composite Materials: Engineering and Science, Boca Raton, CRC (2006).
- [4] S.-M. Choi and H. Awaji, Nanocomposites-a new material design concept, *Sci. Technol. Adv. Mater.* 6 (2005) 2-10.
- [5] K. U. Kainer, Basics of Metal Matrix Composites, in *Metal Matrix Composites*, K. U. Kainer, Ed. Wiley-VCH Verlag GmbH & Co. KGaA, (2006) 1-54
- [6] D. B. Miracle, Metal matrix composites – From science to technological significance, *Compos. Sci. Technol.* 65 (2005) 2526-2540.

- [7] K. KChawla, *Composite Materials: Science and Engineering*, Springer Science & Business Media, New York (2012).
- [8] C. Suryanarayana, E. Ivanov, and V. V. Boldyrev, The science and technology of mechanical alloying, *Mater. Sci. Eng.* A304-306 (2001) 151-158.
- [9] C. Suryanarayana, Mechanical alloying and milling, *Prog. Mater. Sci.*, 46 (2001) 1-184.
- [10] D. Balzar and H. Ledbetter, Voigt-function modeling in Fourier analysis of size- and strain-broadened X-ray diffraction peaks, *J. Appl. Crystallogr.*, 26 (1993) 97-103.
- [11] D. Balzar, N. Audebrand, M. R. Daymond, A. Fitch, A. Hewat, J. I. Langford, A. Le Bail, D. Louër, O. Masson, C. N. McCowan, N. C. Popa, P. W. Stephens, and B. H. Toby, Size-strain line-broadening analysis of the ceria round-robin sample, *J. Appl. Crystallogr.*, 37 (2004) 911-924.
- [12] C. C. Koch, Materials Synthesis by Mechanical Alloying, *Annu. Rev. Mater. Sci.*, 19(1989)121-143.
- [13] B. S. Murty, M. Mohan Rao, and S. Ranganathan, Milling maps and amorphization during mechanical alloying, *Acta Metall. Mater.*, 43 (1995) 2443-2450.
- [14] T. Raghu, R. Sundaresan, P. Ramakrishnan, and T. R. Rama Mohan, Synthesis of nanocrystalline copper-tungsten alloys by mechanical alloying, *Mater. Sci. Eng.* A304-306 (2001) 438-441.
- [15] F. T. Wallenberger, Commercial and Experimental Glass Fibers, in *Fiberglass and Glass Technology*, F. T. Wallenberger and P. A. Bingham, Eds., US, Springer, (2010) 3-90.
- [16] G. Zak, M. N. Sela, V. Yevko, C. B. Park, and B. Benhabib, Layered-Manufacturing of Fiber-Reinforced Composites, *J. Manuf. Sci. Eng.*, 121 (1999) 448-456.
- [17] C. L. Schutte, Environmental durability of glass-fiber composites, *Mater. Sci. Eng. RRep.*, 13 (1994) 265-323.
- [18] T. W. Chou, A. Kelly, and A. Okura, Fibre-reinforced metal-matrix composites, *Composites*, 16 (1985) 187-206.
- [19] J. R. Brockenbrough, S. Suresh, and H. A. Wienecke, Deformation of metal-matrix composites with continuous fibers: geometrical effects of fiber distribution and shape, *Acta Metall. Mater.*, 39 (1991) 735-752.
- [20] B. Budiansky, J. W. Hutchinson, and A. G. Evans, Matrix fracture in fiber-reinforced ceramics, *J. Mech. Phys. Solids*, 34 (1986) 167-189.
- [21] J. E. Bolander, S. Choi, and S. R. Duddukuri, Fracture of fiber-reinforced cement composites: effects of fiber dispersion, *Int. J. Fract.*, 154 (2008) 73-86.
- [22] V. Srinivasa, V. Shivakumar, V. Nayaka, S. Jagadeeshaiah, M. Seetharam, R. Shenoy, and A. Nafidi, Fracture morphology of carbon fiber reinforced plastic composite laminates, *Mater. Res.*, 13 (2010) 417-424.
- [23] Q. Du, M. Perez, W. J. Poole, and M. Wells, Numerical integration of the Gibbs–Thomson equation for multicomponent systems, *Scr. Mater.*, 66 (2012) 419-422.
- [24] I. McCue, J. Snyder, X. Li, Q. Chen, K. Sieradzki, and J. Erlebacher, Apparent Inverse Gibbs-Thomson Effect in Dealloyed Nanoporous Nanoparticles, *Phys. Rev. Lett.*, 108(2012) 225-503.